Available online at www.sciencedirect.com

SCIENCE DIRECT®

Int. J. Miner. Process. 75 (2005) 53–68

INTERNATIONAL JOURNAL OF MINERAL PROCESSING

www.elsevier.com/locate/ijminpro

CFD modelling of hydrocyclone—prediction of cut size

M. Narasimha*, R. Sripriya, P.K. Banerjee

R&D Division, Tata Steel, Jamshedpur, Jharkhand 831007, India

Received 23 October 2003; received in revised form 29 February 2004; accepted 6 April 2004

Abstract

The flow behavior in hydrocyclone is quite complex. This complexity of flow processes has led designers to rely on empirical equations for predicting the equipment performance. The publications on empirical models of the hydrocyclone far out-number few fluid-flow-modeling attempts. Empirical models correlate a classification parameter, such as the cut-size, with device dimensions and slurry properties. However, these can only be used within the extremes of the experimental data from which the model parameters were determined. On the other hand, models based on Computational Fluid Dynamics (CFD) techniques have proven to be useful in simulating fluid flow in hydrocyclones, and in predicting the separation efficiency of solid particles in the separator for a wide range of operating and design conditions. The shape and size of a hydrocyclone separator has a direct influence on the internal flow structure of the continuous phase and, thereby, the separation of the particulate phase. Hydrocylcones usually have a single inlet that distributes the feed stream near the end wall between the vortex finder and the sidewall. Effect of spigot diameter, i.e., 10 and 20 mm and inlet water velocities (5.91–12.35 m/s) on the water splits and particle classification in the hydrocyclone have been studied. The cut size of the hydrocyclone, operated at very low pulp density, has been predicted using discrete phase modeling technique. The studies revealed that with an increase in feed flow rate and decrease in spigot diameter the cyclone sharpness of separation improves. These predictions were found similar in line with the experimental observations.

Keywords: hydrocyclones; computational fluid dynamics; Navier–Stokes equation; particle trajectory; standard $k-\varepsilon$ model; discrete phase model; particle slip velocities; separation efficiency curve

1. Introduction

Since the Second World War, there has been a rapid growth in the use of hydrocyclones in the chemical, mineral, coal and powder-processing industries. The reasons for this popularity lie in the design and operational simplicity, high capacity, low maintenance and operating cost and the small physical size of the device.

A typical hydrocyclone consists of a cylindrical section with a central tube connected to a conical section with a discharge tube. An inlet tube is attached to the top section of the cylinder. The fluid being injected tangentially into hydrocyclone causes swirling and thus generates centrifugal force within the device. This centrifugal force field brings about a rapid classification of particulate material from the medium in which it is suspended.

The flow behavior in hydrocyclone is quite complex. This complexity of flow processes has led designers to rely on empirical equations for predicting the equipment performance. These empirical relationships

* Corresponding author. Fax: +91-657-2271510.
E-mail address: narasimha.mangadoddy@tatasteel.com (M. Narasimha).

0301-7516/$ - see front matter © 2004 Elsevier B.V. All rights reserved.
doi:10.1016/j.minpro.2004.04.008

are derived from an analysis of experimental data and include the effect of operational and geometric variables. Different sets of experimental data lead to different equations for the same basic parameters. Empirical models correlate a classification parameter, such as the cut size, with device dimensions and slurry properties (Dahlstrom, 1949; Yoshiota and Hotta, 1955; Fahlstrom, 1963; Agar and Herbst, 1966; Lynch and Rao, 1975; Plitt, 1976). However, these models suffer from the inherent deficiency as any other empirical models—the model can only be used within the extremes of the experimental data from which the model parameters were determined. In view of this shortcoming, mathematical models based on fluid mechanics are highly desirable.

Computational Fluid Dynamics (CFD) is a versatile means to predict velocity profiles under a wide range of design and operating conditions. The numerical treatment of the Navier–Stokes equations are the backbone of any CFD technique gradually crept into the analysis of the hydrocyclone in the early 1980s. This resulted from the rapid improvement in computers and a better understanding of the numerical treatment of turbulence.

2. Modelling and hydrocyclones—an overview

Bloor and Ingham (1987) applied the Navier–Stokes equation to compute the flow field in hydrocyclones and gave an analytical solution, with overly simplifying assumptions. In the region near the central axis, the vortex conservation was applied, with inviscid and rotational flow assumptions, which yields axial and radial components. In the region along the wall, the boundary-layer approach was used to derive velocities. Despite Bloor and Ingham's efforts in predicting velocity data measured by Kelsal (Kelsal, 1952), a data set often referred to in numerous publications, the lack of an adequate turbulence description led others to revise the analytical solutions as necessary. The first successful work in predicting the fluid flow in hydrocyclones is that of Pericleous and Rhodes (1986) and Pericleous et al. (1984), who used the PHOENICS computer code for the solution of the partial differential equations. Using the simple Prandtl mixing length model and the axisymmetry assumptions, the authors reported the velocity predictions in a 200-mm hydrocyclone. Later, Hsieh and Rajamani (1991) numerically solved the turbulent momentum equations to obtain the velocities and compared them with the Laser Doppler Velocimetry measurements in a 75-mm hydrocyclone. This work showed that, by a simple balance of forces on a particle present in the flow field, the trajectory of the particle can be traced inside the hydrocyclone, from which the entire size-classification efficiency is computed. In a sequel, Monredon et al. (1990) showed that the same model is evidently applicable even if the vortex finder and spigot dimensions were changed drastically, besides the operating conditions. All of these modeling works have been confined to hydrocyclones processing slurries in the 5–10% solids range, and have mostly been restricted to axisymmetric geometries (Boysan et al., 1982; Davidson, 1988). The practical constraints in carrying out 3D simulations have been the allocable memory and the total amount of CPU time that may be spent on the simulation. However, a few three-dimensional simulations have been reported in recent years (Cristea et al., 1994; Slack and Wraith, 1997; Hoekstra et al., 1999).

Most of these studies have aimed to simulate only the flow of water in a hydrocyclone; very few attempts have been made to predict the flow of solids in the separator. An attempt has been made in this study to predict both water and solids splits in a laboratory hydrocyclone. The model predictions were also compared with experimental results.

3. Theoretical considerations

3.1. Modelling water flow—turbulence models

For a dilute fluid suspension, the incompressible Navier–Stokes equations supplemented by a suitable turbulence model are appropriate for modelling the flow in a hydrocyclone. The most popular turbulence model in use for engineering applications is the k–ε model where the scalar variables k and ε represent the kinetic energy of turbulence and its dissipation rate, respectively. These following equations describe the steady-state conservation of mass and momentum,

$$\nabla \cdot (\rho \overrightarrow{v}) = 0 \tag{1}$$

$$\nabla \cdot (\rho \overrightarrow{v}\overrightarrow{v}) = -\nabla p + \nabla \cdot (\bar{\tau}) + \rho \overrightarrow{g} \tag{2}$$

where p is the static pressure, $\rho\bar{g}$ is the gravitational body force. $\bar{\bar{\tau}}$ is the stress tensor given by,

$$\bar{\tau} = \mu_{\text{effective}}\left[\left(\nabla \overrightarrow{v}\right) - 2/3\,\nabla \cdot \overrightarrow{v}I\right] \quad (3)$$

where $\mu_{\text{effective}} = \mu + \mu_t$.

To start with, the standard $k-\varepsilon$ model was used to represent the turbulence in the equipment. The model was used to predict the water flow rates in the two outlet streams for different inlet velocities of water.

3.1.1. The standard k–ε model

The standard $k-\varepsilon$ model is a semi-empirical model based on model transport equations for the turbulent kinetic energy (k) and its dissipation rate (ε), and are given by

$$\frac{\partial}{\partial t}(\rho k) + \frac{\partial}{\partial x_i}(\rho k u_i) = \frac{\partial}{\partial x_j}\left[\left(\mu + \frac{\mu_i}{\sigma_k}\right)\frac{\partial k}{\partial x_j}\right] + G_k - \rho\varepsilon \quad (4)$$

$$\frac{\partial}{\partial t}(\rho \varepsilon) + \frac{\partial}{\partial x_i}(\rho \varepsilon u_i) = \frac{\partial}{\partial x_j}\left[\left(\mu + \frac{\mu_t}{\sigma_\varepsilon}\right)\frac{\partial k}{\partial x_j}\right] + C_{1\varepsilon}\frac{\varepsilon}{k}(G_k) - C_{2\varepsilon}\rho\frac{\varepsilon^2}{k} \quad (5)$$

$$G_k = -\rho\overline{u_i' u_j'}\,\frac{\partial u_j}{\partial x_i} \quad (6)$$

In these equations, G_k represents the generation of turbulent kinetic energy due to the mean velocity gradients, $C_{1\varepsilon}$, $C_{2\varepsilon}$ and $C_{3\varepsilon}$ are constants. σ_k and σ_ε are the turbulent Prandtl numbers for k and ε, respectively. The 'eddy'' or turbulent viscosity, μ_t defined in Eqs. (2) and (3) can be computed by combining k and ε as follows:

$$\mu_t = \rho C_\mu \frac{k^2}{\varepsilon} \quad (7)$$

where C_μ is a constant.

The model constants $C_{1\varepsilon}$, $C_{2\varepsilon}$, C_μ, σ_k and σ_ε were assumed to have the following values: $C_{1\varepsilon}$=1.44, $C_{2\varepsilon}$=1.92, C_μ=0.09, σ_k=1.0, σ_ε=1.3.

3.2. Modelling of solids movement using discrete phase modeling

In this modeling technique, the second phase is introduced as a discrete phase that can be simulated in a Lagrangian frame of reference by defining the initial position, velocity and size of individual particles. This second phase consists of spherical particles dispersed in the continuous phase. The initial conditions, along with the inputs defining the physical properties of the discrete phase, are used to initiate trajectory calculations. The trajectory calculations are based on the force balance on the particle, using the local continuous phase conditions as the particle moves through the flow. The formulation contains the assumption that the second phase is sufficiently dilute that particle–particle interactions and the effects of the particle volume fraction on the continuous phase are negligible.

3.2.1. Particles in turbulent flows

The dispersion of particles due to turbulence in the fluid phase was predicted using the stochastic tracking model. The stochastic tracking (or ''random walk'') model includes the effect of instantaneous turbulent velocity fluctuations on the particle trajectories through the use of stochastic methods. The particles are assumed to have no direct impact on the generation or dissipation of turbulence in the continuous phase.

3.2.2. Equations of motion for particles

The trajectory of the discrete phase particle is obtained by integrating the force balance on the particle, which can be written in a Lagrangian reference frame. This force balance equates the particle inertia with the forces acting on the particle, and can be written (for the x direction in Cartesian coordinates) as

$$\frac{\mathrm{D}u_\mathrm{p}}{\mathrm{d}t} = F_\mathrm{D}(u - u_\mathrm{p}) + g\left(\frac{\rho_\mathrm{p} - \rho_\mathrm{l}}{\rho_\mathrm{p}}\right) + F_x \quad (8)$$

where $F_\mathrm{D}(u_p - u)$ is the drag force per unit particle mass and

$$F_\mathrm{D} = \left(\frac{18\mu D_\mathrm{p}^2}{\rho_\mathrm{p}}\right)\left(\frac{C_\mathrm{D}Re}{24}\right) \quad (9)$$

Here, u is the fluid phase velocity, u_p is the particle velocity, μ is the molecular viscosity of the fluid, ρ_l is the fluid density, ρ_p is the density of the particle and D_p is the particle diameter Re is the relative Reynolds number which is defined as

$$Re = \frac{\rho D_p (u_p - u)}{\mu}. \tag{10}$$

The values of the drag coefficient, C_D, can be obtained from the literature. For submicron particles, a form of Stoke's drag law is available and in that case F_D is defined as

$$F_D = \frac{18\mu}{\rho_p} D_p^2 C_c \tag{11}$$

where $C_c = 1 + \{2\lambda/D_p \lfloor 1.257 + 0.4\exp(-1.1(D_p/2\lambda))\rfloor\}$, where λ is the mean free path.

4. Experimental aspects

4.1. Numerical method

The studies were carried out in a laboratory hydrocyclone of 101 mm diameter. The computational grid was set up in Cartesian coordinate, as shown in Fig. 1. Since it is difficult to represent tangential inlet conditions in two dimensions, the study was carried out in three dimensions. Velocity inlet boundary condition at the inlet and pressure boundary conditions (outlet gauge pressure equals to zero) were applied to the two outlets. The physical constants of the liquid phase were set to those of water.

The flow of water through the hydrocyclone was modelled using a CFD package FLUENT 6. A detailed discussion of the numerical method and several validation studies of this code are given by Mathur and Murthy (1997). In this code, the domain is discretized into arbitrary unstructured polyhedra. The discretized form of the governing equations for each cell is obtained such that the conservation principles are obeyed on each polyhedron. The resulting discretized equations for the variable φ are given by:

$$a_p \phi_p = \sum a_{nb} \phi_{nb} + S_p \tag{12}$$

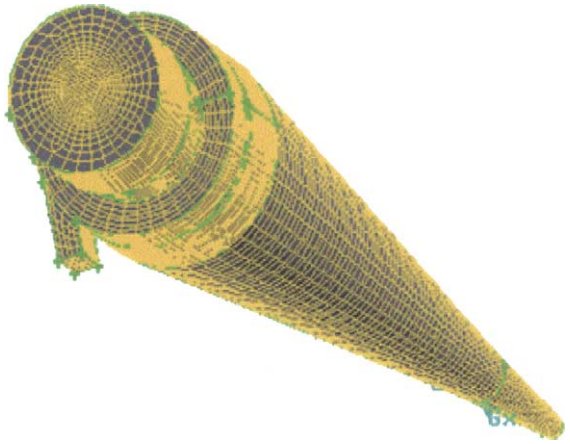

Fig. 1. Meshed hydrocyclone geometry (diameter: 101 mm, vortex finder: 35 mm and spigot: 10 mm).

The summation in the above equation extends over all the neighbour cells of cell p, i.e., all the cells, which share a face with the cell p. The number of cell neighbours in Eq. (1) is arbitrary for unstructured meshes. Therefore, normal line-iterative solvers cannot be used. In FLUENT, the linear equations are solved using an algebraic multigrid procedure developed by Hutchinson and Raithby (1986). It uses colocated meshes considering their well-known advantages over staggered meshes for complex geometries. Checker-boarding of pressure and velocity fields on the collocated meshes is avoided by a momentum interpolation procedure. The SIMPLE algorithm is used for coupling the continuity and momentum equations. All the results presented in this section are obtained using a third-order accurate QUICK scheme for spatial discretization (Patankar, 1980).

4.2. Laboratory tests

Laboratory tests were carried out with a cyclone having geometry identical to the one used for the computational work as shown in Fig. 2. In any cyclone due to the tangential entry, an outer spiral is created which changes direction in the conical partition of cyclone, moves upward pulling the finer particles with it. This inner vortex envelopes an air core (visible clearly in Fig. 2) which is a negative pressure of zero velocity region. The vortex finder

Fig. 2. Laboratory hydrocyclone (diameter: 101 mm, vortex finder 35 mm and spigot: 10 mm).

was kept constant at 35 mm. Two spigot diameters of 10 and 20 mm were used during the studies. The inlet water flow rate was varied during the tests. From each experiment, timed samples were collected from the overflow and underflow streams. The collected samples were weighed and mass flow rates determined. The same was used to determine the water splits in the product streams.

The ultimate aim of the modeling effort is to predict the size classification achieved in the hydrocyclone. The classification of a hydrocyclone is commonly represented by partition curve, which represents the percentage of each particle size of the feed reporting to over flow against the particle size.

To determine the partition curve of the cyclone, pure sand was collected, washed and then ground in a ball mill to below 75 μm for the classification tests. Since it is difficult to trace few number of particles in an actual hydrocyclone test, the tests were conducted at low pulp density of the sand–water mixture. The tests were conducted at 1.6% (by weight) pulp density. During each test, timed samples of overflow and underflow products were collected, weighed, filtered and dried. The dried samples were then weighed and subjected to size analysis in a Frietz micro-sieve shaker. The weights of dry solids of each size fraction was noted and the same was used to construct the partition curve of the separator (Banerjee et al., 2002). The actual cut size (d_{50}) of the sand was determined from the partition curve and the same was compared with the predicted value.

4.3. Particle size classification prediction

The flow of solids in a hydrocyclone was modelled using discrete particle model (DPM) available in the FLUENT software. Pure sand particles of 2.6 specific gravity and different sizes (below 75 μm) were used for the studies. All the simulation runs were carried out for two different spigot diameters, i.e., 10, 20 mm at different inlet water velocities, varying from 5.95 to 12.35 m/s for 10 mm apex diameter and from 5.95 to 11.4 m/s for 20 mm apex diameter hydrocyclones. Before particle tracking, simulation was conducted with single phase, i.e., water, to determine the velocity distribution of water inside the cyclone. Then, sand particles of uniform size were injected through the inlet of the separator and their flow paths within the cyclone were tracked. The outlet stream in which the each particle reported was noted and the separation characteristics of the cyclone were determined. Each run was repeated five times and the average value was noted. During each run, 1050 particles of same size were injected simultaneously. Simulation runs were repeated for sand particles of different size. These data were then used to generate the partition curve of the cyclone and to predict the cut size (d_{50}). The model predictions were compared with the experimental results obtained for similar conditions.

The geometric dimensions of the two hydrocyclones studied are listed in Table 1.

Table 1

Dimensions	Cyclone 1 (case 1)	Cyclone 2 (case 2)
Cyclone diameter, mm	101	101
Inlet entry, mm	25 × 12.5	25 × 12.5
Cylindrical length, mm	85	85
Vortex finder diameter, mm	35	35
Vortex finder length, mm	50	50
Spigot diameter, mm	10	20
Cone angle, °	20	20

Cyclone 1 is considered as the base case. Cyclone 2 is studied for variation on the spigot diameter.

5. Results–discussions

5.1. Modelling the water flow

The computations were carried out for two different spigot diameters, i.e., 10, 20 mm at different inlet water velocities, varying from 5.95 to 12.35 m/s for 10 mm apex diameter and from 5.95 to 11.4 m/s for 20 mm apex diameter hydrocyclones. For inlet velocity of 9.5 m/s of 10 mm apex diameter hydrocyclone, the velocity distributions of water at the exit points of overflow and underflow are shown in Figs. 3 and 4,

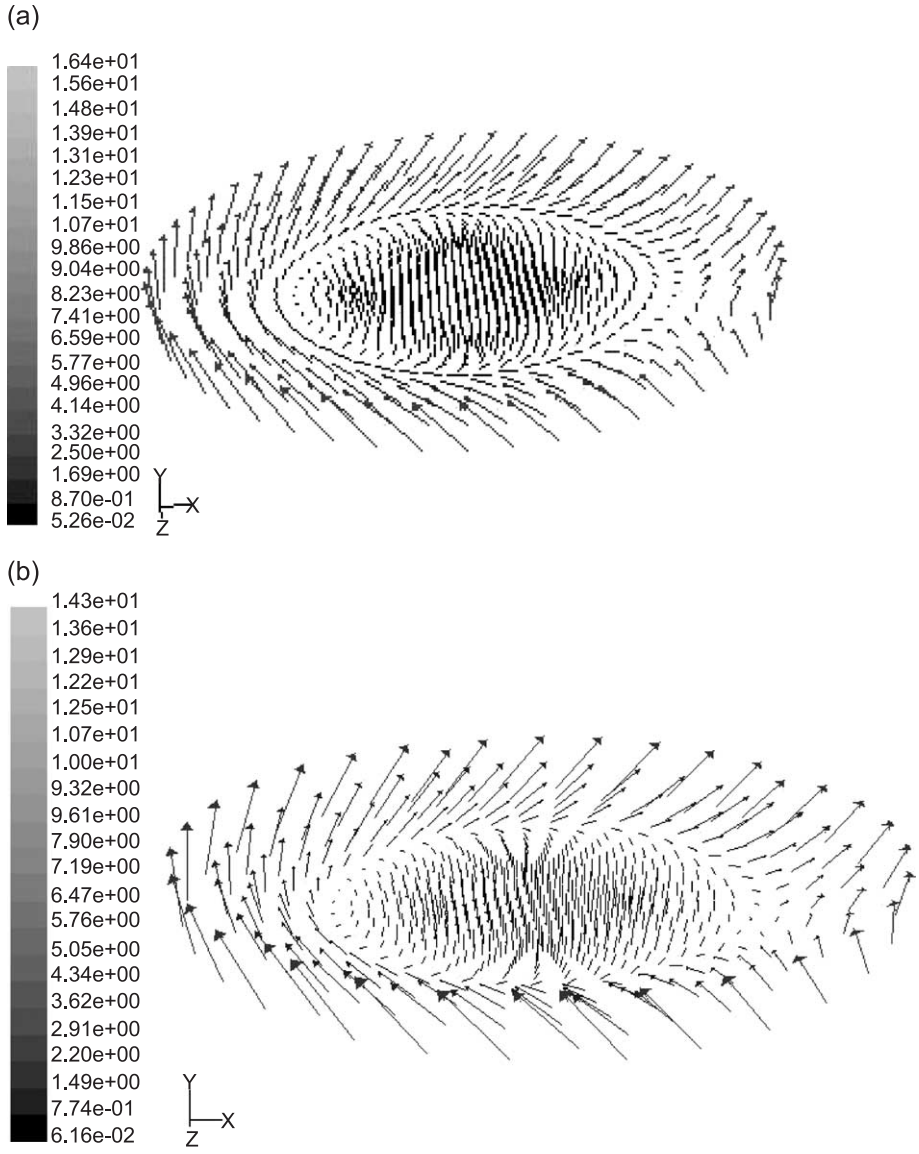

Fig. 3. (a and b) Comparison of velocity vectors in the overflow of the hydrocyclone for inlet velocity of 9.5 m/s for two different spigots of 10 and 20 mm, respectively.

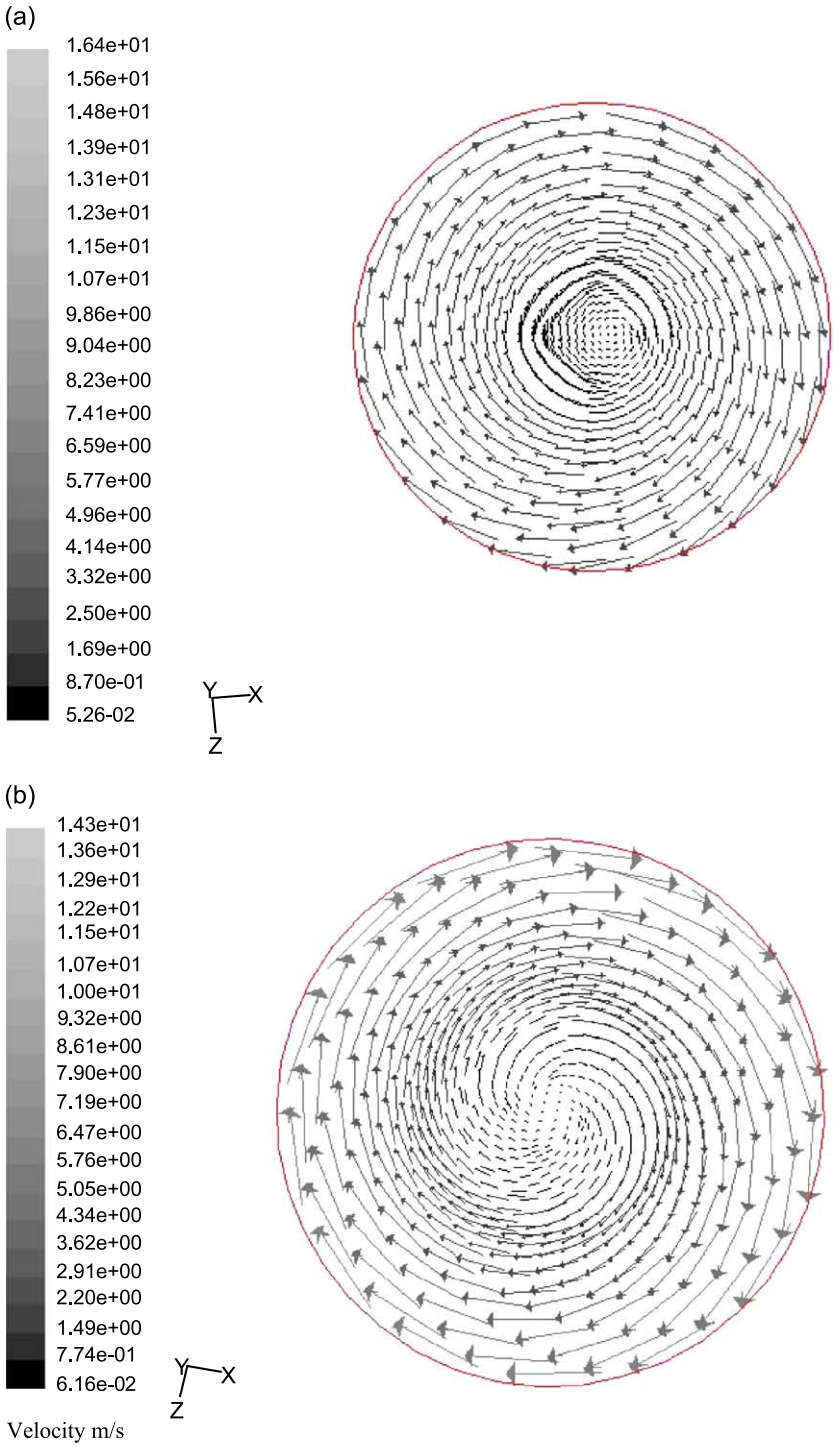

Fig. 4. (a and b) Comparison of velocity vectors in the underflow of the hydrocyclone for inlet velocity of 9.5 m/s for two different spigots of 10 and 20 mm, respectively.

respectively. Fig. 4 clearly shows an umbrella type water discharge from the spigot of the hydrocyclones. The figures also show that the secondary swirling patterns are more occupied in 10 mm spigot compared to 20 mm spigot hydrocyclone, the same was also observed during laboratory experimentation. The predicted velocity distribution was used to compute the mass fluxes at the outlets. The predicted mass flow rates and water split into vortex finder along with the corresponding experimental values are presented in Table 2 for 10 mm apex diameter hydrocyclone. It is interesting to note from the table that the predicted results match very well with the experimental values ($\pm 0.5\%$ error). The results for 20 mm apex diameter are shown in Table 3.

Typical flow patterns at the interior portion as well as at different planes (xz) are shown in Figs. 5 and 6. The figures show clearly the two parallel swirling patterns, i.e., one is near the wall side and the another one is the secondary one which moves towards the over flow outlet side. It is interesting to note that a central very low velocity zone is created due to high swirling motion of water inside the cyclone. Hydrocyclones usually develop an air core because the swirl generates a region of negative gauge pressure along the axis. In fact the entire central low velocity zone represents the actual air core formation in the cyclone as shown in Fig. 2. A multi-phase modelling study might be needed to predict the exact interface of air–water inside the hydrocyclone which would be the future scope of work. The velocity vectors points upwards towards the vortex, near the outlet.

5.1.1. Velocity field near the inlet

Figs. 7 and 8 show the velocity field at the horizontal level where the inlet pipe enters the hydrocyclone. The graphs indicate the deviation from axisymmetry in this region that is shown clearly in the contour graph for the swirl intensity. The swirl contours are the magnitude of the circumferential (tangential) component of the velocity and it exhibits significant deviation form axisymmetry. These results indicate the importance of a complete three-dimensional calculation of the hydrocyclone flow fields. In these figures, the magnitude of the tangential velocity is high at the inlet entry and gradually decreases as it moves in radially, and it gains some momentum at rear portion of the inlet because of the ventury fluid expansion of the inlet get in the cyclone.

5.1.2. Velocity field along the center-plane

Figs. 9 and 10 as shown below are the velocity distributions along the center-plane which bisects the hydrocyclone vertically across its inlet opening. The velocity vector plot displays some of the minor flow patterns in the hydrocyclone flow field. A recirculation zone exists beneath the inlet region is seen clearly in the velocity vector plot. The fluid is seen flowing downward along the hydrocyclone wall and the flow direction reverses along the lower part of the conical section. The upward fluid flow is moving rapidly near the central air core. The contour graph for the circumferential velocity component shows high swirl levels both at the outer and inner rims of the hydrocyclone. The swirl movements are reversed between the outer and inner zones.

Table 2
Comparison of predicted water splits with experimental values in a 101-mm hydrocyclone (apex diameter 10 mm)

Test no.	Inlet velocity, m/s	Predicted values			Experimental values			Deviation (error) for water split in VF, %
		Inlet flow rate, kg/s	VF flow rate, kg/s	Water split into VF, %	Inlet flow rate, kg/s	VF flow rate, kg/s	Water split into VF, %	
1	6.1	1.903	1.876	98.58	1.896	1.865	98.36	−0.22
2	9.5	2.963	2.934	99.02	2.966	2.940	99.12	0.10
3	11.35	3.540	3.512	99.21	3.868	3.850	99.53	0.32
4	12.35	3.850	3.820	99.22	3.868	3.850	99.53	0.31
5	10.70	3.337	3.309	99.16	3.378	3.325	98.43	−0.73
6	8.25	2.574	2.544	98.83	2.604	2.563	98.42	−0.41
7	5.91	1.844	1.816	98.48	1.937	1.894	97.78	−0.70

Table 3
Comparison of predicted water splits with experimental values in a 101-mm hydrocyclone (apex diameter 20 mm)

Test no.	Inlet velocity, m/s	Predicted values			Experimental values			Deviation (error) for water split in VF, %
		Inlet flow rate, kg/s	VF flow rate, kg/s	Water split into VF, %	Inlet flow rate, kg/s	VF flow rate, kg/s	Water split into VF, %	
1	7.05	2.200	1.865	85.68	2.201	1.84	83.60	−2.08
2	7.40	2.308	1.969	85.31	2.305	1.92	83.30	−2.01
3	9.40	2.932	2.585	88.17	2.941	2.55	86.71	−1.46
4	11.03	3.441	2.955	85.87	3.480	3.036	87.24	1.37
5	11.4	3.556	3.201	90.01	3.565	3.14	88.08	−1.93
6	10.73	3.347	2.743	81.95	3.513	2.967	84.45	2.49
7	5.95	1.856	1.417	76.34	1.948	1.543	79.21	2.87

5.1.3. Flow characteristics

The experimental results shows, the water split factor (water split into vortex finder, %) changed from 98.42% for Cyclone 1 to 84.45% for Cyclone 2 for an inlet flow velocity of 10.7 m/s. The numerical results show these values to be around 99.16% for Cyclone 1 and 81.95 % for Cyclone 2 for the same inlet velocity. The upward axial velocity decreases when the spigot diameter is increased. The spigot diameter can be varied to control the underflow rate.

5.2. Modelling the flow of solid particles

5.2.1. Particle separation

Accurate prediction for the particle separation performance is the ultimate goal in a hydrocyclone modeling study. In the following calculations, around

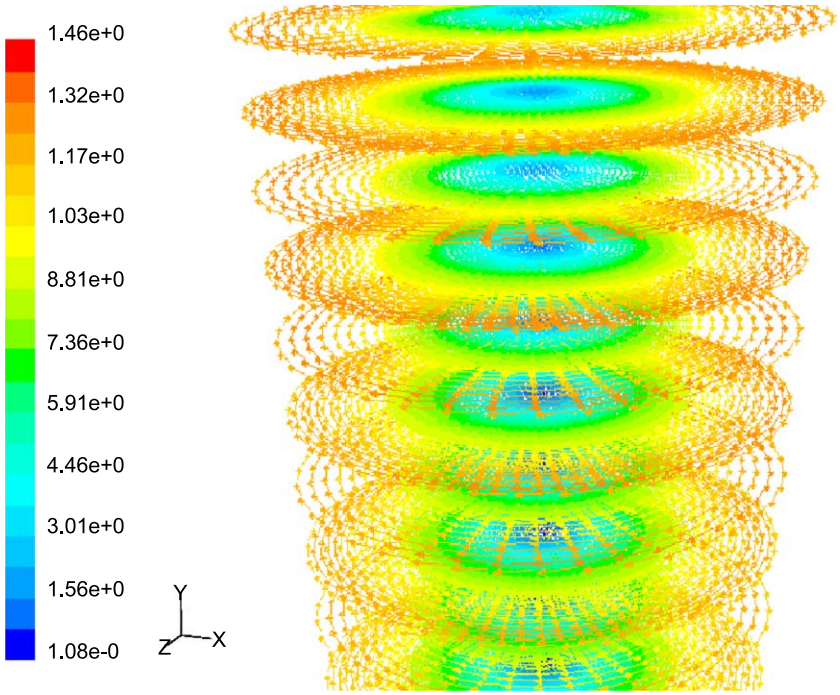

Fig. 5. Figure showing velocity patterns in the hydrocyclone of spigot 20 mm.

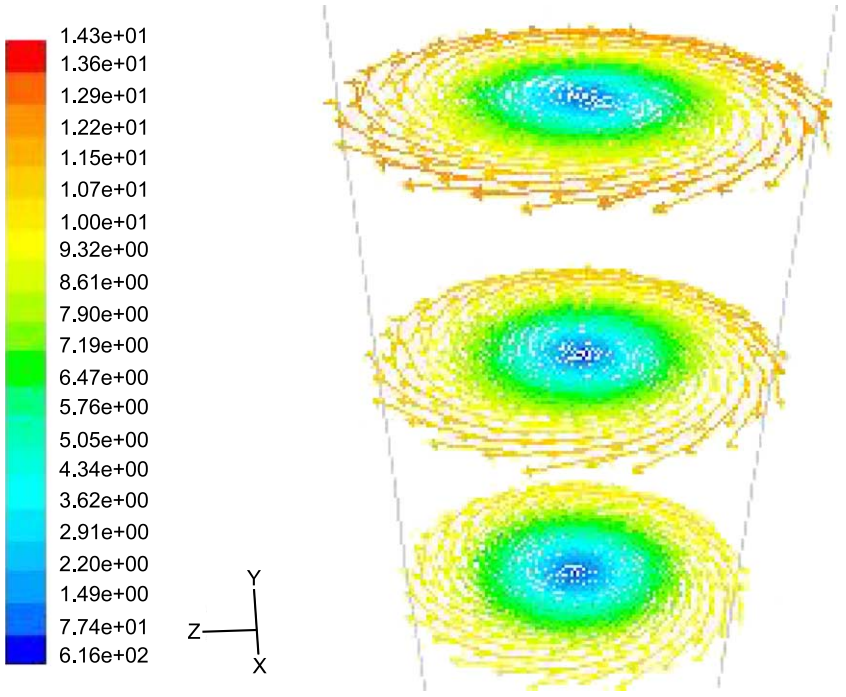

Fig. 6. Figure showing the velocity patterns in different planes (at 0.45, 0.4, 0.35 m height) of hydrocyclone of spigot 20 mm.

1050, sand particles are initially distributed randomly at the flow inlet and are transported by the flow field until they either leave through the overflow or the underflow opening. Then a different particle size is assigned and repeated for a range of particle sizes (1–75 μm). These data were then used to calculate the partition coefficient, i.e., the probability of given size particle to report to overflow product. To verify the model predictions, actual experiments were carried out in the laboratory hydro-

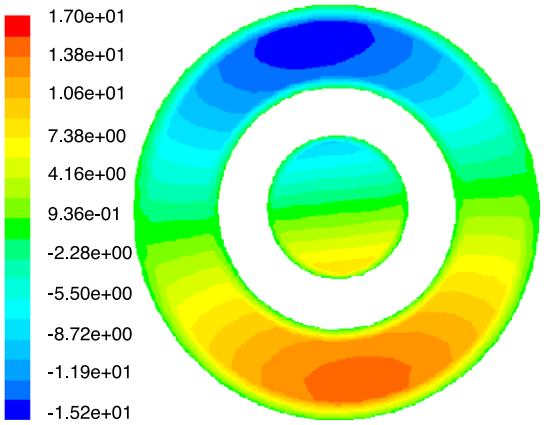

Fig. 7. Figure showing swirl velocity contours at the inlet in the hydrocyclone of spigot 10 mm (10.70 m/s).

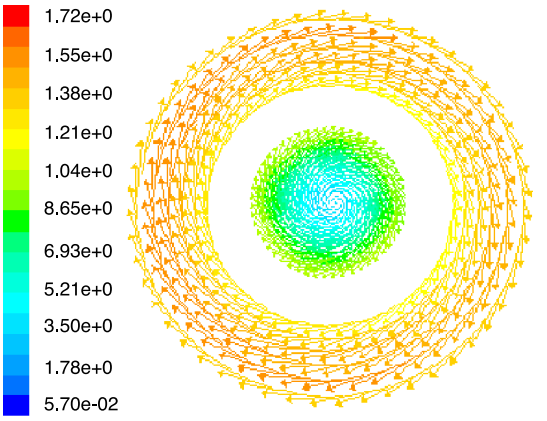

Fig. 8. Figure showing the velocity vectors inlet in the hydrocyclone of spigot 10 mm (10.70 m/s).

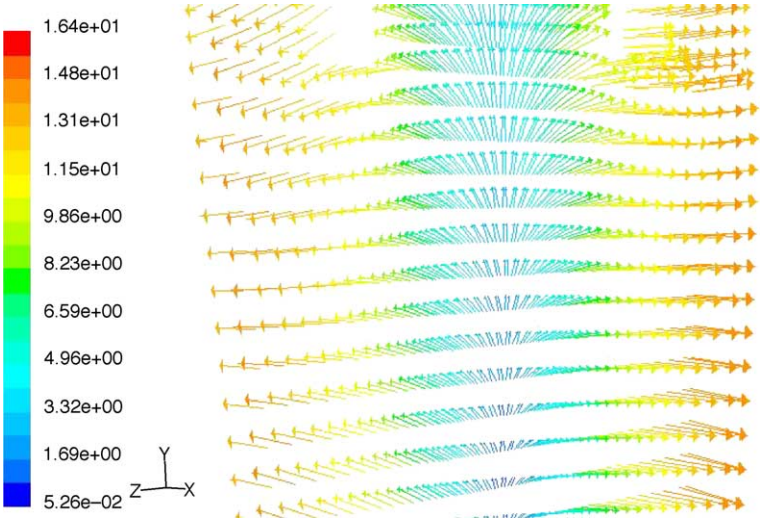

Fig. 9. Velocity vectors in the center axial–radial plane.

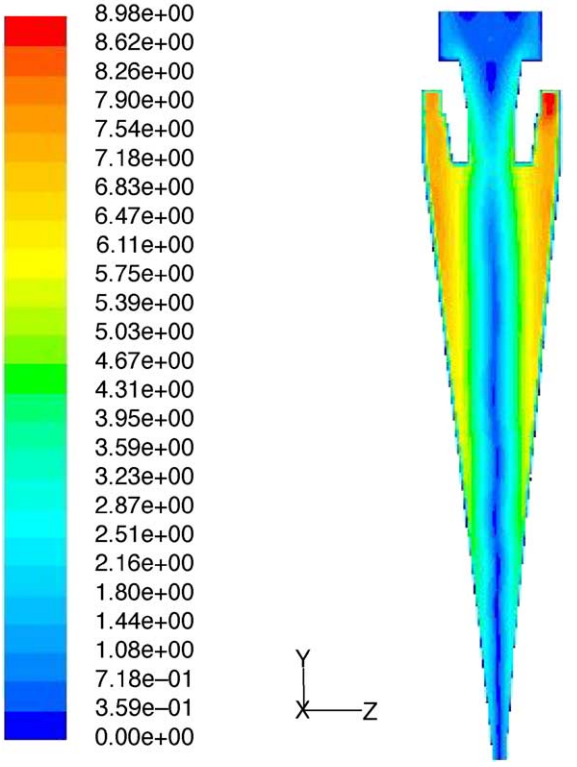

Fig. 10. Tangential velocity contours in the center axial–radial plane.

cyclone under similar conditions at different pulp densities.

Most of (80% of solids) the particles coarser than 30 μm are classified to the underflow. The classification of particles in the range between 7.5 and 30 μm is size dependent and as particle size decreases, more particles flow to the overflow. The particles having size of 1 μm are completely reporting to overflow only.

The partition curves shows (from Figs. 11–14) that the predictions are all over predicted compared to experimental values. The apparent over-prediction of the computed collection efficiencies for the larger particles may be due to the occurrence of turbulent bursts in the wall boundary layer which may cause parcels of particles to shoot in the radial direction towards the axis of the cyclone, and to re-entrainment of particles from the vortex finder.

5.2.2. The effect of inlet flow rate

Since the operating variables have an important effect on the cyclone performance, it is necessary to study the effect of inlet flow rate on the efficiency of cyclone. As shown in Tables 1 and 2, it is clear that as the inlet flow rate increases the water splits will increase through the vortex-finder as well as spigot outlets. Since the capacity of cyclone will increase as the feed rate increases.

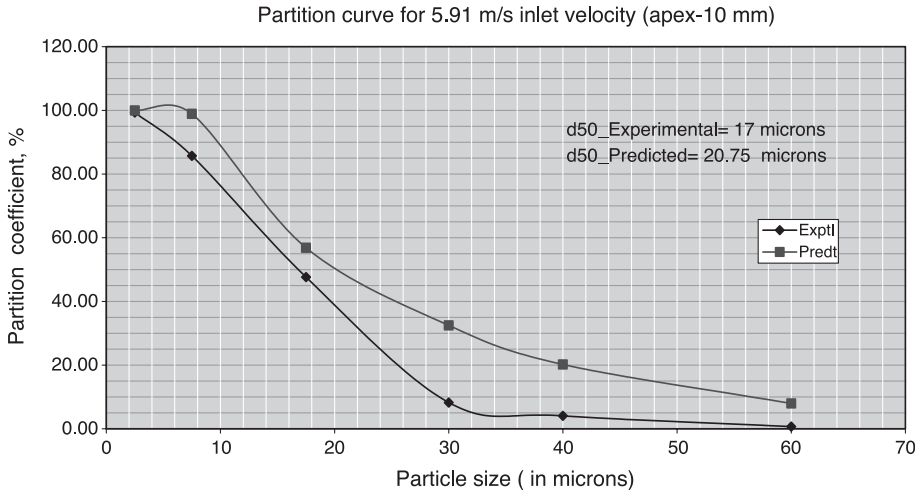

Fig. 11. Comparison of partition curves at 5.91 m/s inlet velocity (spigot 10 mm).

It has been observed from Figs. 15 and 16 that an increase in feed flow rate will improve efficiency by increasing the centrifugal force on particles. Since increase in feed rate, or pressure drop, increases the centrifugal force effect, finer particles are carried to underflow, and d_{50} is decreased, but the change has to be large to have a significant effect. The studies revealed that with an increase in feed flow rate the cyclone sharpness of separation improves.

5.2.3. The effect of spigot diameter

The partition curves for 10 and 20 mm spigot diameter 4-in. hydrocyclone are shown in Fig. 17. From the predictions, it has been observed that when the spigot diameter increases, the efficiency drops for both coarse and fine particles. The drop in efficiency for fine particles is due to the increase in the water underflow split ratio. When spigot diameter is enlarged a greater portion of the inflow fluid reports to the underflow, which carries with it more particles in each

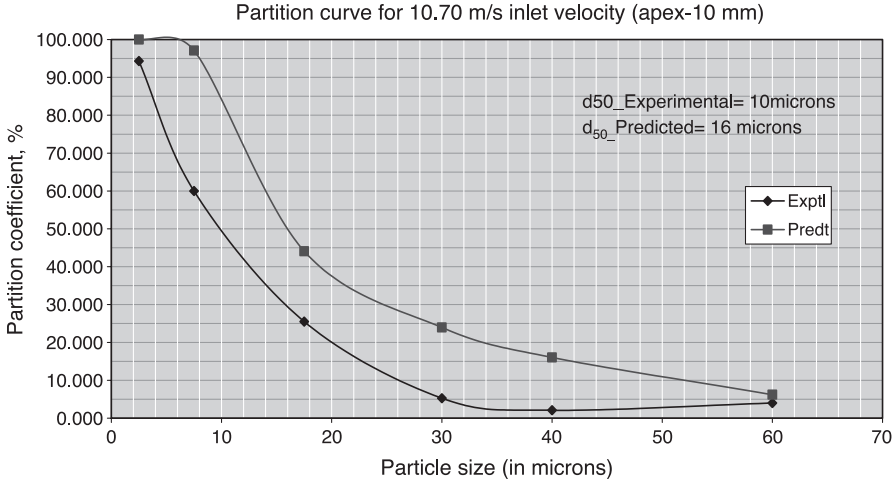

Fig. 12. Comparison of partition curves at 10.70 m/s inlet velocity (spigot 10 mm).

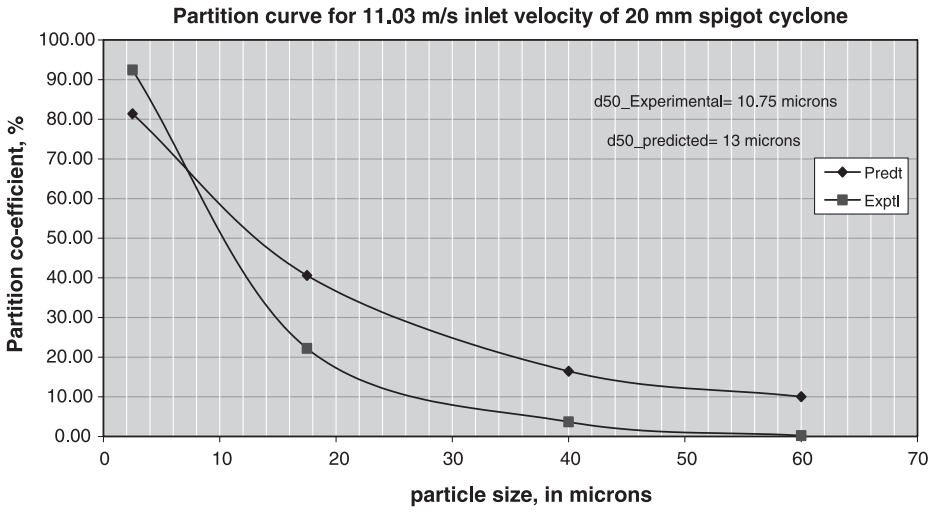

Fig. 13. Comparison of partition curves at 11.03 m/s inlet velocity (spigot 20 mm).

class. In addition to the fluid split effect, the crowding effect plays a role in the classification of coarse particles. Crowding effect refers to the crowding of particles between the air core and conical wall especially near the spigot region. For 20 mm spigot cyclone, because of the increase in the tangential velocities, the flow of solids along the conical wall increases. The bulk volume of solids in the spigot region becomes greater than the solids capacity of the spigot pipe, hence a portion of the coarse particle is

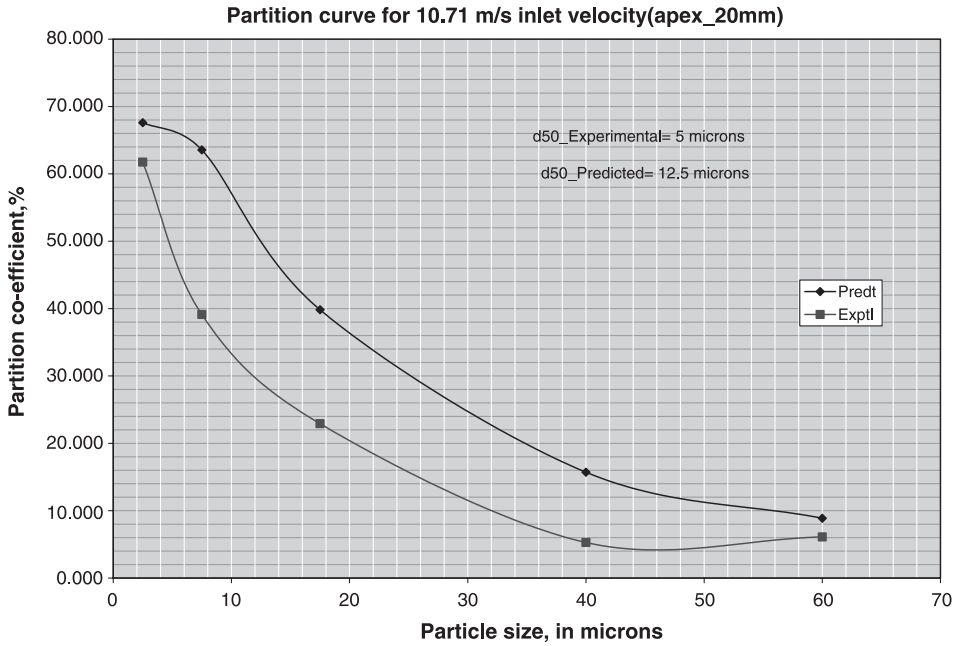

Fig. 14. Comparison of partition curves at 10.71 m/s inlet velocity (spigot 20 mm).

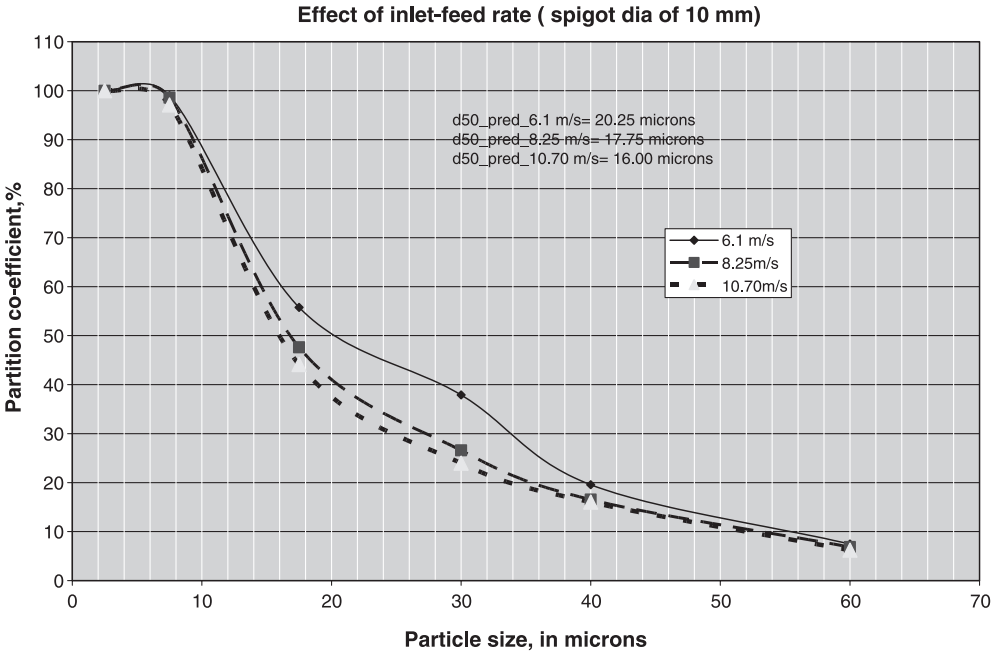

Fig. 15. Comparison of partition curves for 10 mm spigot hydrocyclone.

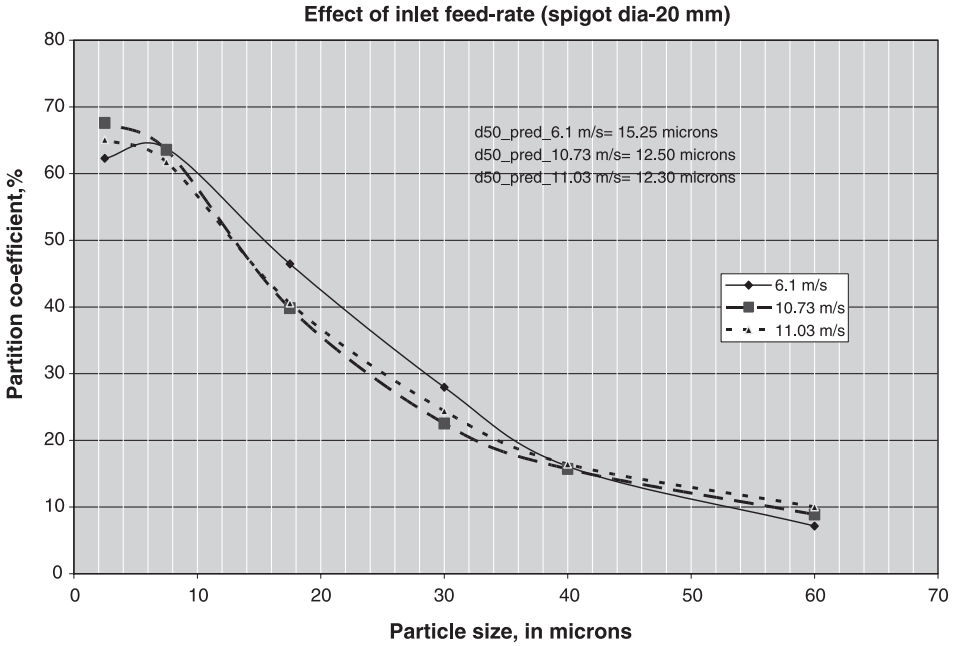

Fig. 16. Comparison of partition curves for 20 mm spigot hydrocyclone.

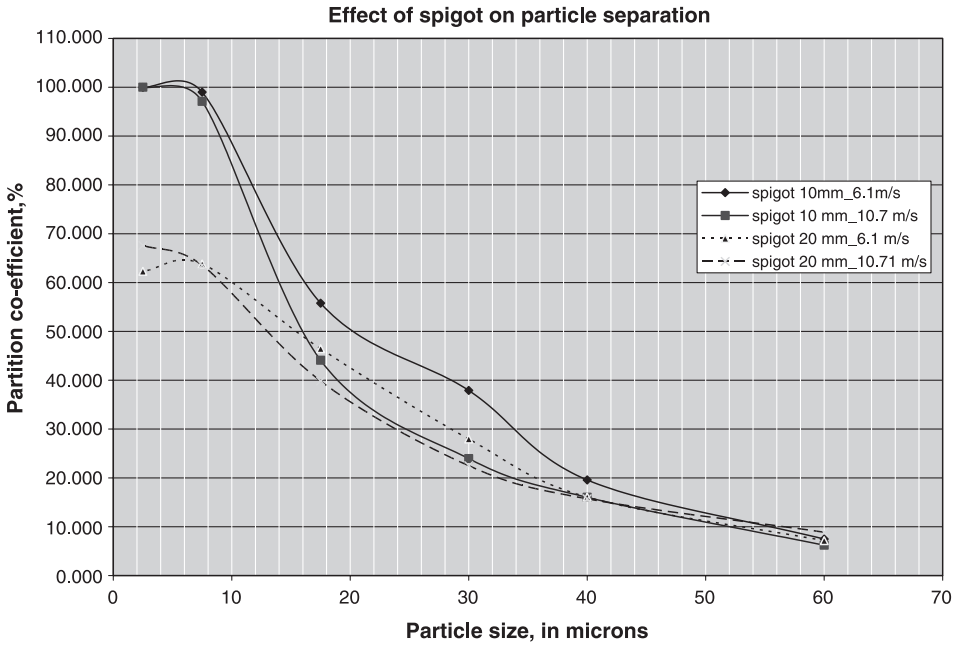

Fig. 17. Comparison of partition curves for different spigot hydrocyclones.

carried upward to the overflow. The saturation in the spigot region is responsible for the decrease in the efficiency and corresponding decrease in the cut-size. The studies revealed that with decrease in spigot diameter the cyclone sharpness of separation improves.

6. Conclusions

CFD technique has great potential in understanding the fluid flow behaviour in a hydrocyclone. Flow of water through a laboratory hydrocyclone has been studied using FLUENT package. The predicted water splits in the outlets for various inlet water velocities were in good agreement with the experimental results. As a first step towards predicting the classification of the hydrocyclone, discrete phase modeling technique was attempted.

It has been observed that most of (80% of solids) the particles coarser than 30 μm are classified to the underflow. The classification of particles in the range between 7.5 and 30 μm is size dependent, and as particle size decreases, more particles flow to the overflow. The particles having a size of 1 μm are completely reporting to overflow only.

An increase in feed flow rate will improve efficiency by increasing the centrifugal force on particles, and d_{50} is decreasing. It has been observed that when the spigot diameter increased, the efficiency drops for both coarse and fine particles. The cut size for pure sand particles as predicted from the model was reasonably in good agreement for classification at low pulp density. Prediction of particle classification using discrete phase modelling technique is encouraging.

List of symbol

μ	Molecular viscosity of the fluid
ε	Dissipation rate of the turbulent kinetic energy
λ	Mean free path
σ_k and σ_ε	the turbulent Prandtl numbers for k and ε, respectively
ρ_l	Density of the liquid
ρ_m	Pulp density of the slurry by wt.%
ρ_p	Density of the particle
φ_p	Variable φ for all cells p
μ_t	Turbulent eddy viscosity
$C_{1\varepsilon}$, $C_{2\varepsilon}$, $C_{3\varepsilon}$, C and C_c	constants
C_D	Drag coefficient

D/dt	Substantial derivative u fluid phase velocity
D_p	Diameter of the particle
$F_D(u_p - u)$	Drag force
F_x	Additional forces like buoyancy, etc., acting on the particle
G_b	Generation of turbulent kinetic energy due to buoyancy
G_k	Generation of turbulent kinetic energy due to the mean velocity gradients
g_x	Acceleration due to gravity
k	Turbulent kinetic energy
R	Radius of the hydrocyclone
S_p	Source term
u_p	Particle velocity
U_s	Axial slip velocity of the particle
V	Tangential velocity of the fluid
W_s	Radial slip velocity of the particle
Y_M	Contribution of the fluctuating dilatation in compressible turbulence to the overall dissipation rate

Acknowledgements

The authors would like to express their sincere thanks to Dr. O.N. Mohanty and Dr. S. Chandra for their keen interest and encouragement for undertaking these studies.

References

Agar, G.E., Herbst, J.A., 1966. The effect of fluid viscosity on cyclone classification. Soc. Min. Eng., 145–149 (June).

Banerjee, P.K., Sripriya, R., Mar, 2002. Fluid flow modeling of hydrocycolnes. R&D Internal Report No: R&D/RC/EXP/02/01/50/01, R&D, Tata Steel, India.

Bloor, M.I.G., Ingham, D.B., 1987. The flow in industrial cyclones. J. Fluid Mech. 178, 507–519.

Boysan, F., Ayers, W.H, Swithenbank, J., 1982. A fundamental mathematical modelling approach to cyclone design. Trans. Ichem. E. 60, 222–230.

Cristea, E.D, Malfa, E., Coghe, A., 1994. 3D simulation and experiments of cement rotary kiln preheater top cyclone. Fluent Users Group Meeting UK.

Dahlstrom, D., 1949. Cyclone operating factors and capacities on coal and refuse slurries. Trans. Am. Inst. Min. Eng. 184, 331–344.

Davidson, M.R., 1988. Numerical calculations of flow in a hydrocyclone operating without an air core. Appl. Math. Model. 12, 119–128.

Fahlstrom, P.H., 1963. Studies of the hydrocyclone as a classifier. In: Roberts, A. (Ed.), Proc. 6th Int. Miner. Process. Congr., Cannes. Pergamon, London, pp. 87–112.

Hoekstra, A.J., Derksen, J.J., Van den Akker, H.E.A., 1999. An experimental and numerical study of turbulent swirling flow in gas cyclones. Chem. Eng. Sci. 54, 2055–2065.

Hsieh, K.T., Rajamani, R.K., 1991. A mathematical model of the hydrocyclone based on physics of fluid flow. AIChE J. 37, 735–746.

Hutchinson, B.R., Raithby, G.D., 1986. A multigrid method based on the additive correction strategy. Numer. Heat Transf. 9, 511–537.

Kelsal, D.F., 1952. A study of the motion of solid particles in a hydraulic cyclone. Trans. Inst. Chem. Eng. 30, 87–108.

Lynch, A.J., Rao, T.C., 1975. Modeling and scale-up of hydrocyclone classifiers. In: Carta, M. (Ed.), Proc. 11th Int. Miner. Process. Congr., Cagliari. Aziende Tipografiche Bardi, Rome, pp. 245–269.

Mathur, S.R., Murthy, J.Y., 1997. A pressure-based method for unstructured meshes. Numer. Heat Transf., Part B Fundam. 31, 195–215.

Monredon, T.C, Hsieh, K.T., Rajamani, R.K., 1990. Fluid flow model of the hydrocyclone: an investigation of device dimensions. Int. J. Miner. Process. 35, 65–83.

Patankar, S.V., 1980. Numerical Heat Transfer and Fluid Flow. Hemisphere Publishing, New York.

Pericleous, K.A, Rhodes, N., 1986. The hydrocyclone classifier—a numerical approach. Int. J. Miner. Process. 17, 23–43.

Pericleous, K.A., Rhodes, N., Cutting, G.W., 1984. A mathematical model for predicting the flow field in a hydrocyclone classifier. Proc. Int.Conf. Hydrocyclones. Bath, England, pp. 27–38.

Plitt, I.R., 1976. A mathematical model of the hydrocyclone classifier. CIM Bull., 114–123.

Slack, M.D., Wraith, A.E., 1997. Modelling the velocity distribution in a hydrocyclone. 4th Int. Colloq. on Process Simulation, Helsinki university of technology, Espoo, Finland, 65–83.

Yoshiota, N., Hotta, Y., 1955. Liquid cyclone as a hydraulic classifier. Chem. Eng. Jpn. 19 (12), 632–640.